CENTRAL ASIAN TRANSACTIONS ON MATERIALS STRUCTURE AND PROPERTIES

Vol. 1, Issue 1, June 2026.

https://doi.org/10.51885/3134-7983_CATMSP_2026_2_6
SRSTI 53.39.31

SYNTHESIS OF COBALT-FREE HIGH-STRENGTH WC-BASED CEMENTED CARBIDES BY SPARK PLASMA SINTERING

Nurken Mussakhan [1], **Aray Abdimutalip** [1*], **Sardor Kambarbekov** [1], **Dilnoza Baltabayeva** [1], **Berik Kaldar** [1]

[1]The Research Institute "Natural Sciences, Nanotechnology and New Materials", Khoja Akhmet Yassawi International Kazakh-Turkish University, Turkestan, Kazakhstan
* Corresponding author: Aray Abdimutalip, e-mail: aray.abdimutalip@ayu.edu.kz

Keywords:
Tungsten carbide, Fe-Ni binder, Spark plasma sintering, microstructure, X-ray diffraction, EDS mapping.

ABSTRACT
This study investigates the effect of spark plasma sintering (SPS) temperature (1250 °C and 1300 °C) on the microstructure, phase composition, porosity, density of cobalt-free WC–Fe–Ni, WC–Fe, and WC–Ni hard alloys. The aim of the work was to evaluate the potential of Fe- and Fe–Ni-based binders as alternatives to cobalt in cemented carbides for cutting-tool applications. Microstructural analysis revealed that the WC–Fe–Ni alloy formed a homogeneous and dense structure with a uniform distribution of WC particles at 1250 °C, while increasing the sintering temperature to 1300 °C resulted in carbide grain refinement. In contrast, the WC–Fe system exhibited grain coarsening at the higher temperature. The WC–Ni alloy was characterized by large irregular grains and the formation of brittle secondary phases. X-ray diffraction analysis confirmed the presence of WC, Fe_3W_3C, $FeNi_3$, and Fe–Ni solid-solution phases in the WC–Fe–Ni system, whereas the WC–Ni alloy was dominated by W_2C and W_3Ni_3C phases. Increasing the SPS temperature reduced porosity from 13.2% to 12.7% in WC–Fe–Ni and from 13.8% to 12.0% in WC–Fe, accompanied by an increase in relative density to approximately 87–88%. In contrast, the WC–Ni alloy exhibited the highest porosity (~16%). The results demonstrate that both binder composition and SPS temperature strongly influence phase evolution, densification, and microstructural development. Fe-containing binders provided greater structural homogeneity and phase stability, highlighting their potential as cobalt-free alternatives for cemented carbide applications.

INTRODUCTION

Enhancing the performance properties of materials and products, along with extending their operational lifetime, represents one of the most critical challenges in modern materials science. In this context, intensive research is underway into alloys and protective coatings that can offer high wear resistance, strength, and thermal stability under severe operating conditions. Among such materials, cemented carbides based on tungsten carbide hold a special position, being widely utilized across various industries to protect tools and structural components of machinery (Aghaali et al., 2023; Huang et al., 2025; Zhong et al., 2016). Consequently, these alloys find applications in numerous fields, including metallurgy, medicine, transport, aerospace, as well as in the production of excavator teeth and other parts of earthmoving equipment (Buravlev et al., 2021; Ma et al., 2019; Maizza et al., 2018). In cemented carbides, tungsten carbide serves as the primary hard phase, imparting high hardness and wear resistance to the alloy. At the same time, the material exhibits considerable crack resistance, reaching about 15–20 MPa·$m^{1/2}$ (Cai et al., 2019; Heydari et al., 2012; Ren et al., 2025). Thanks to the combination of these attributes, such materials can be employed to protect components operating under extreme conditions, including parts of nuclear power plants, where high temperatures and significant thermal loads may occur. Traditionally, cobalt is used as the metallic binder in cemented carbides, playing a key role in wetting tungsten carbide particles and forming a robust metallic matrix. This enhances the material's flexural strength, achieving 3–4 GPa. This, in turn, contributes to the improved strength and stability of refractory hard alloys based on WC. Moreover, iron can form stable carbide phases that are thermodynamically stable and promote the refinement of tungsten carbide grains, which positively affects the material's mechanical properties. Ni-Fe alloys are widely adopted in industry owing to their good corrosion resistance and relatively low cost (Gao et al., 2018; Jin et al., 2022; Soria-Biurrun et al., 2023). With an optimal choice of chemical composition and processing parameters, such materials can exhibit properties comparable to, or even exceeding, those of conventional cobalt-based binder systems.

A variety of technological techniques are employed to produce these alloys, including laser remelting, vacuum melting, conventional sintering, and other powder metallurgy approaches. However, the optimal balance of strength and hardness is typically achieved through modern sintering methods, with spark plasma sintering (SPS) being particularly noteworthy. SPS relies on the application of pulsed electric current, which activates compaction and reactive sintering processes in powder materials. Compared to conventional methods such as hot pressing, hot isostatic pressing, induction heating, or liquid-phase sintering, this technology enables high material density to be attained at lower temperatures and within substantially shorter processing times (Chang et al., 2015).

Although considerable attention has been devoted to the development of cobalt-free WC-based cemented carbides, a systematic comparison of Fe-, Ni-, and Fe–Ni-bonded systems processed under identical SPS conditions remains limited. In particular, the influence of binder composition on phase evolution, microstructure development, and hardness at different SPS temperatures has not been fully clarified. Furthermore, the potential of Fe–Ni binders as a cost-effective and environmentally friendly alternative to conventional cobalt binders requires further investigation. Therefore, the novelty of the present work lies in the comparative study of WC–Fe, WC–Ni, and WC–Fe–Ni cemented carbides fabricated by SPS at different sintering temperatures. Special attention is given to the relationship between binder composition, phase formation, microstructural evolution, and hardness, as well as to the assessment of Fe–Ni binders as potential substitutes for cobalt in cutting-tool applications.

The objective of this work is to fabricate cobalt-free WC-(FeNi), WC–Fe, and WC–Ni cemented carbide systems using SPS and to investigate their phase composition, morphology, hardness, and physical–mechanical properties.

MATERIALS AND METHODS

In this study, tungsten carbide (WC), nickel (Ni), and iron (Fe) with a purity of 99% and a particle size of less than 50 μm, supplied by Hebei Suoyi New Material Technology (Hebei Province, China), were used as starting powder materials. The preparation of powder mixtures included a mechanical activation step. The mechanical activation process and detailed experimental procedure were previously described in our previous work (Aidarova et al., 2025). The mechanosynthesis conditions used in the experiments are given in Table 1.

Table 1. Modes for Mechanosynthesis WC-FeNi, WC-Fe, WC-Ni and composition of powder mixture (Aidarova et al., 2025)

Sample name	Unique code	Time, hour	Surfactant additive (stearic acid), wt%	Rotation speed, rpm	Atmosphere	Mass ratio, (ball/powder)
Powder mixture blending	a	0,3	-	200	Argon	10:1
Mechanosynthesis						
88 wt% WC - 12 wt.%Fe	b1	1	2.5	500	Argon	10:1
	c1	2				
	d1	4	3			
88 wt% WC - 12 wt% Ni	b2	1	2.5			
	c2	2				
	d2	4	3			
88 wt% WC - 6 wt% Fe + 6 wt% Ni	b3	1	2.5			
	c3	2				
	d3	4	3			
Note – compiled by the authors						

After mechanical activation, the resulting powder mixtures were subjected to SPS consolidation using a Dr. Sinter SPS-625 system. The powder mixture was loaded into a 20 mm diameter graphite mold and pre-compacted under a load of 200 kg at a heating rate of 100 °C/min. Sintering was carried out at temperatures of 1250°C and 1300°C with a 5-minute hold, followed by cooling to room temperature over 50 minutes. Three samples with different mass fractions of the components were analyzed; their compositions are presented in Table 2.

Table 2. Sintering conditions for samples using the SPS method

Samples	Composition (wt%)	Temperature °C	Holding time (min)
Alloy 1	88 wt.% WC+6 wt.% Fe+6 wt.% Ni	1250	5
Alloy 2	88 wt.% WC+6 wt.% Fe+6 wt.% Ni	1300	
Alloy 3	88 wt.% WC+12 wt.% Fe	1250	
Alloy 4	88 wt.% WC+12 wt.% Fe	1300	
Alloy 5	88 wt.% WC+12 wt.% Ni	1300	
Note – compiled by the authors			

A Tescan Vega 4 scanning electron microscope (SEM) with a thermionic tungsten cathode was used to accurately examine the sample and obtain detailed surface images. Surface details, phase types, and structural characteristics of the powders were analyzed using an X-ray diffractometer (Malvern Panalytical Ltd., Almelo, the Netherlands) with a Cu anode, a 20-90° measurement angle, a 40 kV light-emitting tube voltage, a 30 mA current, a 0.02 step size, and a 2 s measurement time at each step.

RESULTS AND DISCUSSION

XRD patterns of WC-based alloys after various sintering temperature processes. X-ray phase analysis of fine- and coarse-grained composites with different contents of the Fe-Ni binder phase (Fig. 1) showed that samples of WC-Fe-Ni and WC-Fe compositions predominantly consist of Fe, WC and Fe3W3C phases, which is consistent with the data of Lee et al. (2021). At a sintering temperature of 1250°C, WC is the main and most stable carbide phase. However, as the temperature increases to 1300°C, a decrease in the intensity of WC peaks is observed in the WC-Fe-Ni system, which is due to the partial dissolution of tungsten carbide. The released carbon can react with alloy components to form secondary phases such as Fe_3W_3C, W_2C, and free carbon C. Despite possible phase transformations, WC retains key performance advantages: high hardness, high melting point, thermal shock resistance, and oxidation resistance. The formation of a small amount of the brittle η-phase Fe_3W_3C is due to the reaction α-Fe + WC → γ-Fe + Fe_3W_3C. The low intensity of its diffraction peaks is explained by its small volume fraction.

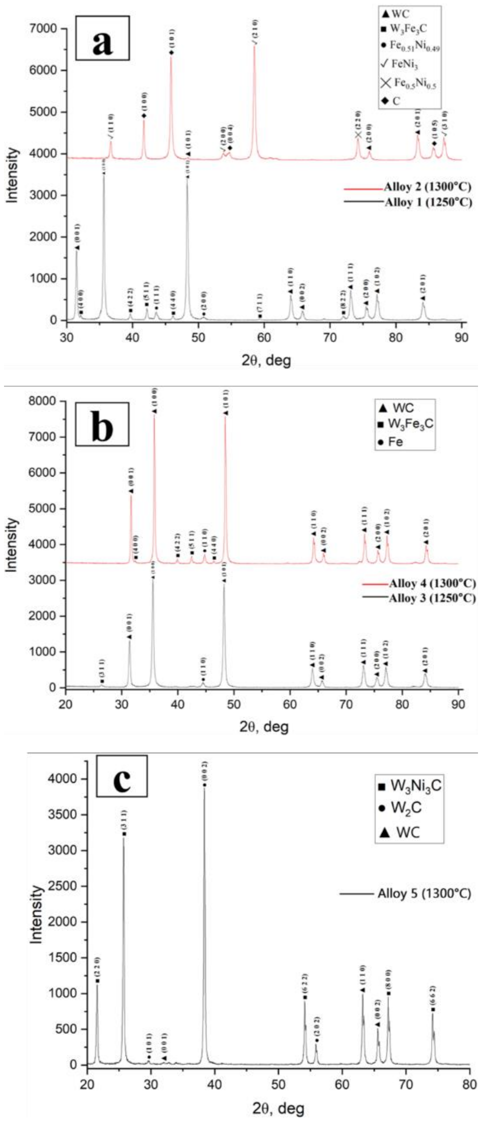

Figure 1. XRD patterns of WC-Fe-Ni cemented carbides with different compositions: (a) Alloy 1,2 (1250 and 1300°C); (b) Alloy 3,4 (1250 and 1300°C); (c) Alloy 5 (1300°C).

Note – compiled by the authors

However, the presence of this phase can weaken the grain boundaries between WC particles and the iron matrix, which potentially reduces the wear resistance of the material (Pan et al., 2019). In the WC-Fe system, an increase in the Fe3W3C content is also associated with SPS features, as noted in Rosa et al. (2020). Under solid-phase sintering conditions at elevated temperatures and short holding times, carbon diffusion is limited, but sufficient for the formation of secondary phases. In WC-Ni samples (Fig. 1c), the subcarbide phase W2C was detected, which promotes grain coarsening, leading to a decrease in hardness and fracture toughness (Cai et al., 2018). The formation of W2C can occur as a result of carbon redistribution during cooling, while the characteristic faceted morphology of WC grains is preserved (Zeng et al., 2025). The introduction of nickel into the WC-Fe-Ni system leads to a decrease in the grain size and deformation of the crystal lattice due to the formation of solid solutions of the Fe0.5Ni0.5 and Fe0.51Ni0.49 types, which is accompanied by the occurrence of internal microscopic stresses. In addition, the formation of the intermetallic phase FeNi3 helps to suppress the formation of the brittle η-phase. The use of a binder phase based on Fe-Ni also improves the corrosion resistance and oxidation stability of the composite (Kurbanbekov et al., 2024). Additionally, it should be noted that under SPS conditions, possible formation of metastable phases such as Ni3C (3Ni + C → Ni3C) and W2C (2WC + 3Ni → W2C + Ni3C) should be noted, which can lead to the formation of η-phases of the Ni3W3C type (da Silva et al., 2021). The formation of Ni3W3C carbide, characterized by a reduced carbon content, is undesirable, since it leads to a significant deterioration in the mechanical properties of the material (Aghaali et al., 2023). It should be noted separately that there is a pronounced diffraction peak of free carbon (C), which may indicate a local redistribution of carbon during the sintering process and its incomplete binding into carbide phases. Morphology and EDS mapping of tungsten carbide samples. The average grain size is 3±1.5 μm. The morphology of the samples is shown in Fig. 2 and was obtained after sintering using the SPS method. As can be seen from Fig. 2a (1250°C), the structure is relatively loose, the tungsten carbide grains are unevenly distributed, and agglomeration areas are observed. The presence of dark "pore" areas indicates an insufficient degree of compaction and incomplete densification at this temperature.

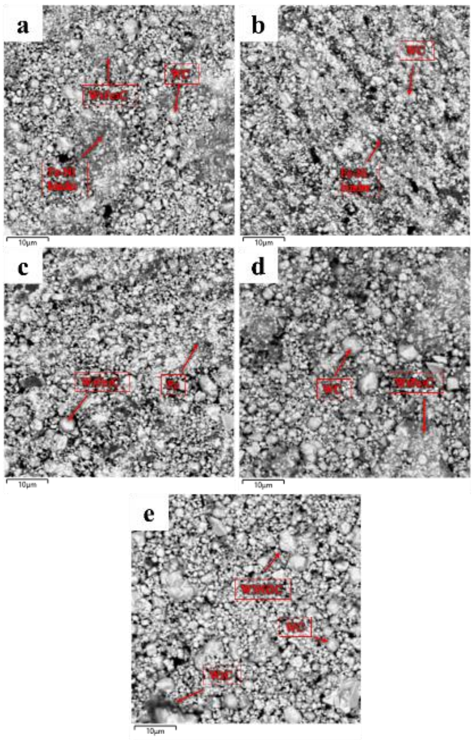

Figure 2. SEM microstructures of the WC-Fe-Ni cemented carbides sintered at different temperatures: (a) Alloy 1 (1250°C); (b) Alloy 2 (1300°C); (c) Alloy 3 (1250°C); (d) Alloy 4 (1300°C); and (e) Alloy 5 (1300°C).

Note – compiled by the authors

In Fig. 2c (1250°C), the structure becomes more uniform compared to Fig. 2a, however, areas with insufficient wetting of the carbide particles by the metal binder remain, indicating limited diffusion and incomplete formation of interphase contacts. With an increase in temperature to 1300°C (Fig. 2b), a pronounced compaction of the structure, a decrease in porosity and an improvement in intergranular cohesion are observed. A more efficient interaction and wetting of tungsten carbide with the iron-nickel binder is noted, which contributes to the formation of a dense composite structure. Fig. 2d (1300°C) shows the growth of WC grains due to the thermal activation of diffusion processes at elevated temperatures, which is consistent with the literature data (Cramer et al., 2020). At the same time, the porosity is significantly reduced compared to the sample obtained at 1250°C (Fig. 2c), indicating a higher degree of sintering. In Fig. 2e (1300°C), the sample with the nickel binder demonstrates the densest and most uniform microstructure. The porosity is minimal, which is associated with the high wetting capacity of nickel and the intensification of diffusion processes at elevated temperatures, which is also confirmed by the results of Aidarova et al. (2025). The intergranular space is effectively filled with the binder, ensuring good adhesion between WC grains and the formation of a uniform composite structure. EDS mapping of the samples obtained at temperatures of 1250 and 1300°C is shown in Fig. 3. WC particles are predominantly rounded and surrounded by a metallic binder based on iron and nickel. This indicates the formation of a binder phase uniformly distributed in the intergranular space and ensuring the formation of a relatively homogeneous composite structure, which is consistent with the results of [23]. The Ni and Fe elements are localized predominantly along the WC grain boundaries, forming a continuous or partially continuous intergranular binder, which promotes structure compaction and improves interparticle contact. At a temperature of 1300°C, a more uniform distribution of the binder elements is observed, which is associated with the intensification of diffusion processes and an increase in the degree of densification. It should be noted that EDS analysis makes it difficult to detect light elements such as carbon (C) and oxygen (O) due to their low sensitivity and overlapping spectral lines. It should be noted that the quantification of light elements, particularly carbon and oxygen, by EDS is associated with higher uncertainty compared with heavier elements such as W, Fe, and Ni. Therefore, the reported C and O contents should be considered semi-quantitative and used primarily for comparative analysis. The measured density of the WC–Fe–Ni alloys increased from 12.39 g/cm3 at 1250 °C to 12.46 g/cm3 at 1300 °C, indicating progressive consolidation during SPS. This behavior can be attributed to enhanced particle rearrangement, neck growth, and diffusion-driven mass transport occurring at elevated temperatures. A comparable trend was observed for the WC–Fe alloys, where the density rose from 12.15 g/cm3 to 12.40 g/cm3 with increasing sintering temperature. The improvement in densification is likely associated with intensified diffusion processes and more effective elimination of residual pores. The WC–Ni alloy exhibited a density of 12.09 g/cm3, which is consistent with its comparatively higher porosity and less compact microstructure. Therefore, their presence is detected primarily in specific zones, particularly in pores or defective areas of the structure. The WC–Fe–Ni composites exhibited a porosity of 13.2% after sintering at 1250 °C. Raising the sintering temperature to 1300 °C resulted in a slight reduction in porosity to 12.7%, indicating enhanced densification of the material. A similar tendency was observed for the WC–Fe system, where porosity decreased from 13.8% at 1250 °C to 12.0% at 1300 °C. These results suggest that higher SPS temperatures promote more efficient particle bonding and consolidation, thereby reducing the volume fraction of pores. In contrast, the WC–Ni alloy sintered at 1300 °C exhibited a porosity of approximately 16%, reflecting a lower degree of densification compared with the Fe-containing systems. The presence of carbon may also be due to the use of graphite fixtures during SPS, which leads to its possible diffusion into the surface layers of the samples. Average atomic and mass percentage values for selected plots are given in table 3a and 3b.

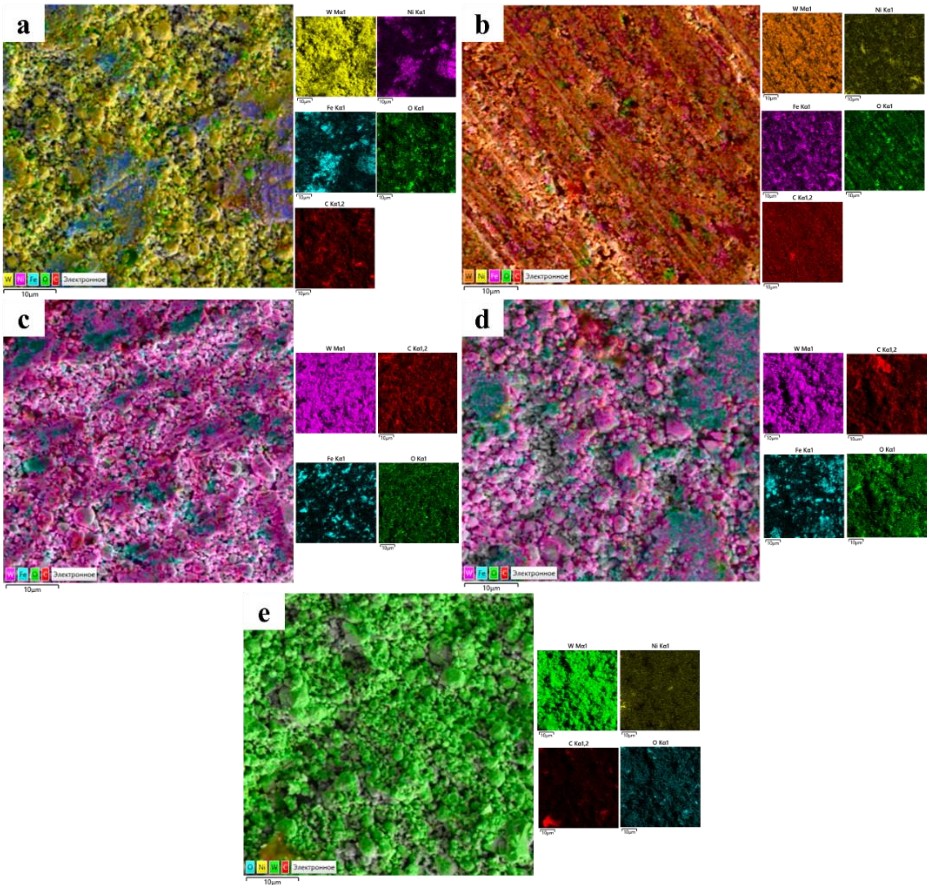

Figure 3. EDS elemental mapping of the alloys after sintering at different temperatures: (a) Alloy 1 (1250°C); (b) Alloy 2 (1300°C); (c) Alloy 3 (1250°C); (d) Alloy 4 (1300°C); and (e) Alloy 5 (1300°C)

Note – compiled by the authors

Table 3a. Average elemental composition (wt.%) derived from EDS maps.

Alloy	WC (wt.%)	Fe (wt.%)	Ni (wt.%)	C (wt.%)	O (wt.%)
Alloy 1	73.75	6.02	5.02	11.84	3.38
Alloy 2	61.82	13.80	3.66	15.74	4.98
Alloy 3	84.66	11.41	0	0	3.93
Alloy 4	70.02	12.69	0	12.71	4.58
Alloy 5	84.24	0.28	0.54	12.90	2.04
Note – compiled by the authors					

Table 3b. Average elemental composition (at.%) derived from EDS maps.

Alloy	WC (at.%)	Fe (at.%)	Ni (at.%)	C (at.%)	O (at.%)
Alloy 1	22.39	6.01	4.77	55.04	11.79
Alloy 2	14.83	10.90	2.75	57.80	13.72
Alloy 3	50.58	22.45	0	0	26.97
Alloy 4	19.51	11.64	0	54.18	14.67
Alloy 5	27.37	0.30	0.55	64.16	7.63
Note – compiled by the authors					

CONCLUSIONS

This study investigated the influence of SPS sintering temperature on the microstructure, phase composition, and morphology of cobalt-free WC-based hardmetals with Fe–Ni, Fe, and Ni binder systems.

Microstructural analysis showed that the WC–Fe–Ni alloy sintered at 1250 °C exhibited a relatively homogeneous and dense structure with a uniform distribution of WC particles within the metallic binder. Increasing the sintering temperature to 1300 °C resulted in microstructural refinement of the carbide phase accompanied by the appearance of localized pores, indicating changes in densification behavior and binder phase redistribution. In the WC–Fe system, higher sintering temperature promoted WC grain growth and the development of a coarser microstructure. EDS analysis revealed the presence of oxygen-containing regions, suggesting partial oxidation of the binder phase at elevated temperature. Increasing the SPS temperature promoted densification in the Fe-containing systems. The porosity of the WC–Fe–Ni alloy decreased from 13.2% to 12.7%, whereas the WC–Fe alloy showed a more significant reduction from 13.8% to 12.0%, accompanied by an increase in relative density to approximately 87–88%. These results indicate improved particle bonding and structural consolidation at higher sintering temperatures. In contrast, the WC–Ni alloy exhibited the highest porosity (~16%), suggesting less effective densification and contributing to its inferior microstructural integrity and mechanical performance.

X-ray diffraction analysis confirmed the formation of WC, Fe_3W_3C, and Fe–Ni phases in the WC–Fe–Ni alloy. Increasing the sintering temperature led to changes in the relative intensities of diffraction peaks and the appearance of additional carbon-containing phases. In the WC–Fe system, WC and Fe_3W_3C remained the dominant phases over the investigated temperature range. In contrast, the WC–Ni alloy was characterized by the formation of W_2C and W_3Ni_3C phases, indicating a different phase evolution pathway compared with the Fe-containing systems.

The results demonstrate that both binder composition and SPS temperature strongly influence the phase evolution, microstructure development, and densification behavior of WC-based hardmetals. Among the investigated compositions, Fe-containing binder systems exhibited higher structural homogeneity and phase stability, whereas the Ni-bonded alloy showed a greater tendency toward the formation of secondary carbide phases. These findings provide useful guidance for the design and optimization of cobalt-free WC hardmetals produced by spark plasma sintering.

CONFLICT OF INTEREST: The authors declare no conflict of interest.

FUNDING: The author(s) declare that financial support was received for the research and/or publication of this article. This research is funded by the Committee of Science of the Ministry of Science and Higher Education of the Republic of Kazakhstan (grant No. BR24992925).

INSTITUTIONAL REVIEW BOARD STATEMENT: Not applicable. The study did not involve human or animal subjects.

INFORMED CONSENT STATEMENT: Not applicable. This research did not involve human participants.

DATA AVAILABILITY STATEMENT: The data supporting the findings of this technical study are available from the corresponding author upon reasonable request.

ACKNOWLEDGEMENTS: We express our gratitude to the Science Committee of the Ministry of Science and Higher Education of the Republic of Kazakhstan. For support of the project “Development of technologies and materials for innovative development of the manufacturing industry of the Republic of Kazakhstan”.

STATEMENT ON THE USE OF ARTIFICIAL INTELLIGENCE TECHNOLOGIES: The authors declare that no artificial intelligence technologies were used in the preparation of this manuscript.

REFERENCES

Huang, N., Guo, S., Ren, H., Guo, J., Li, B., Zhang, J., & Hu, M. (2025). Preparation of V-element-containing Co-based composite powders by spray conversion and its effect on the microstructure properties of cemented carbides. Journal of Alloys and Compounds, 1010, 178273. https://doi.org/10.1016/j.jallcom.2024.178273

Zhong, L., Zhang, X., Chen, S., Xu, Y., Wu, H., & Wang, J. (2016). Fe–W–C thermodynamics and in situ preparation of tungsten carbide-reinforced iron-based surface composites by solid-phase diffusion. International Journal of Refractory Metals and Hard Materials, 57, 42–49. https://doi.org/10.1016/j.ijrmhm.2016.02.001

Aghaali, V., Ebadzadeh, T., Zahraee, S. M., & Mirkazemi, S. M. (2023). Microstructure and mechanical properties of WC–TiC–Co cemented carbides produced by spark plasma sintering (SPS) method. SN Applied Sciences, 5, 285. https://doi.org/10.1007/s42452-023-05510-9

Buravlev, I. Y., Shichalin, O. O., Papynov, E. K., Golub, A. V., Gridasova, E. A., Buravleva, A. A., & Sergienko, V. I. (2021). WC–5TiC–10Co hard metal alloy fabrication via mechanochemical and SPS techniques. International Journal of Refractory Metals and Hard Materials, 94, 105385. https://doi.org/10.1016/j.ijrmhm.2020.105385

Maizza, G., Montanari, R., Richetta, M., Varone, A., Kaciulis, S., Mezzi, A., & Soltani, P. (2018). Surface phenomena during the early stage of liquid phase SPS of a mixture of coarse WC and Ni-alloy particles. Surface and Interface Analysis, 50, 1072–1076. https://doi.org/10.1002/sia.6418

Ma, B., Wang, X., Chen, C., Zhou, D., Xu, P., & Zhao, X. (2019). Dissimilar welding and joining of cemented carbides. Metals, 9, 1161. https://doi.org/10.3390/met9111161

Ren, H. Y., Guo, S. D., Huang, N., Chen, H., Li, B., Guo, J. F., & Wang, B. Q. (2025). Processing of WC-based hard metals using Co–Cr powders obtained by spray conversion. Ceramics International, 51, 15960–15972. https://doi.org/10.1016/j.ceramint.2025.01.432

Cai, X., Zhong, L., Xu, Y., Li, X., & Liu, M. (2019). Microstructure and fracture toughness of a WC–Fe cemented carbide layer produced by a diffusion-controlled reaction. Surface and Coatings Technology, 357, 784–793. https://doi.org/10.1016/j.surfcoat.2018.10.096

Heydari, D., Skandani, A. A., & Al Haik, M. (2012). Effect of carbon content on carbide morphology and mechanical properties of AR white cast iron with 10–12% tungsten. Materials Science and Engineering: A, 542, 113–126. https://doi.org/10.1016/j.msea.2012.02.040

Jin, H., Ji, R., Dong, T., Liu, S., Zhang, F., Zhao, L., & Liu, Y. (2022). Efficient fabrication and characterization of Ni–Fe–WC composite coatings with high corrosion resistance. Journal of Materials Research and Technology, 16, 152–167. https://doi.org/10.1016/j.jmrt.2021.11.145

Soria-Biurrun, T., Lozada-Cabezas, L., Navarrete-Cuadrado, J., Ibarreta-Lopez, F., Martinez-Pampliega, R., & Sanchez-Moreno, J. M. (2023). Densification of WC–Fe–Ni–Co–Cr cemented carbides processed by HIP after sintering: effect of WC powder particle size. International Journal of Refractory Metals and Hard Materials, 110, 105994. https://doi.org/10.1016/j.ijrmhm.2022.105994

Gao, Y., Luo, B. H., He, K. J., Zhang, W. W., & Bai, Z. H. (2018). Effect of Fe/Ni ratio on the microstructure and properties of WC–Fe–Ni–Co cemented carbides. Ceramics International, 44, 2030–2041. https://doi.org/10.1016/j.ceramint.2017.10.148

Chang, S. H., Chang, M. H., & Huang, K. T. (2015). Study on the sintered characteristics and properties of nanostructured WC–15 wt%(Fe–Ni–Co) and WC–15 wt% Co hard metal alloys. Journal of Alloys and Compounds, 649, 89–95. https://doi.org/10.1016/j.jallcom.2015.07.119

Aidarova, M., Kurbanbekov, S., Kizatov, A., Urkunbay, A., Bayatanova, L., Rutkowska-Gorczyca, M., & Amangeldiyeva, Y. (2025). Influence of milling time and binder composition on phase evolution in WC-based composite powders fabricated via high-energy ball milling. Frontiers in Materials, 12, 1684414. https://doi.org/10.3389/fmats.2025.1684414

Lee, J. H., Hong, S. K., & Park, H. K. (2021). Effects of deep cryogenic treatment for tungsten carbide iron cemented carbide. International Journal of Refractory Metals and Hard Materials, 100, 105649. https://doi.org/10.1016/j.ijrmhm.2021.105649

Pan, Y., Liu, A., Huang, L., Du, Y., Jin, Y., Yang, X., & Zhang, J. (2019). Effects of metal binder content and carbide grain size on the microstructure and properties of SPS manufactured WC–Fe composites. Journal of Alloys and Compounds, 784, 519–526. https://doi.org/10.1016/j.jallcom.2019.01.057

Rosa, J. M. B., Lugon, R. D., de Souza Silva, K., das Chagas, V. M., da Silva Guimarães, R., de Carvalho, C. S., & Filgueira, M. (2020). Study of characteristics and properties of spark plasma sintered WC with the use of alternative Fe–Ni–Nb binder as Co replacement. International Journal of Refractory Metals and Hard Materials, 92, 105316. https://doi.org/10.1016/j.ijrmhm.2020.105316

Cai, X., Xu, Y., Liu, M., & Zhong, L. (2018). Evaluation of microstructure and growth kinetics of tungsten carbide ceramics at the interface of iron and tungsten. Journal of Alloys and Compounds, 741, 666–676. https://doi.org/10.1016/j.jallcom.2018.01.212

Zeng, X., Wang, R., Tian, X., & Liu, Y. (2025). Corrosion resistance mechanism in WC/FeCrNi composites: Decoupling the role of spherical versus angular WC morphologies. Metals, 15, 777. https://doi.org/10.3390/met15070777

Kurbanbekov, S., Kozhakhmetov, Y., Skakov, M., Seitov, B., Aidarova, M., & Tabiyeva, Y. (2024). Properties, advantages, and prospects of using cobalt-free composites based on tungsten carbide in industry. Materials, 18, 129. https://doi.org/10.3390/ma18010129

da Silva, E. N., dos Santos, A. A. A., do Nascimento, R. M., Alves, S. M., da Silva Guimarães, R., & Filgueira, M. (2021). Investigation of characteristics and properties of spark plasma sintered ultrafine WC–6.4Fe–3.6Ni alloy as potential alternative WC–Co hard metals. International Journal of Refractory Metals and Hard Materials, 101, 105669. https://doi.org/10.1016/j.ijrmhm.2021.105669

Cramer, C. L., Preston, A. D., Ma, K., & Nandwana, P. (2020). In-situ metal binder-phase formation to make WC–FeNi cermets with spark plasma sintering from WC, Fe, Ni, and carbon powders. International Journal of Refractory Metals and Hard Materials, 88, 105204. https://doi.org/10.1016/j.ijrmhm.2020.105204

Information about authors

Nurken Mussakhan – The Research Institute "Natural Sciences, Nanotechnology and New Materials", Khoja Akhmet Yassawi International Kazakh-Turkish University, Turkestan, Kazakhstan, PhD in Technical Physics, Cobalt-free hard alloys; Microstructure characterization; Physical and mechanical properties of materials
E-mail: nurken.mussakhan@ayu.edu.kz
ORCID: https://orcid.org/0000-0003-4154-0356

Aray Abdimutalip – The Research Institute «Natural Sciences, Nanotechnology and New Materials», Khoja Akhmet Yassawi International Kazakh-Turkish University, Turkestan, Kazakhstan, Second-year master's student, Department of Physics, Spark plasma sintering (SPS); Tungsten carbide-based cemented carbides; Cobalt-free hard alloys
E-mail: aray.abdimutalip@ayu.edu.kz
ORCID: https://orcid.org/0009-0004-0172-2520

Sardor Kambarbekov – The Research Institute «Natural Sciences, Nanotechnology and New Materials», Khoja Akhmet Yassawi International Kazakh-Turkish University, Turkestan, Kazakhstan, Second-year doctoral student, Department of Physics, Spark plasma sintering (SPS); Tungsten carbide-based cemented carbides; Cobalt-free hard alloys
E-mail: sardor.kambarbekov@ayu.edu.kz
ORCID: https://orcid.org/0009-0001-6794-1281

Dilnoza Baltabayeva – The Research Institute «Natural Sciences, Nanotechnology and New Materials», Khoja Akhmet Yassawi International Kazakh-Turkish University, Turkestan, Kazakhstan, Second-year doctoral student, Department of Physics, Spark plasma sintering (SPS); Tungsten carbide-based cemented carbides; Cobalt-free hard alloys
E-mail: dilnoza.baltabayeva@ayu.edu.kz
ORCID: https://orcid.org/0000-0001-8249-4398

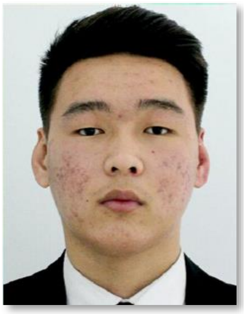

Berik Kaldar – The Research Institute «Natural Sciences, Nanotechnology and New Materials», Khoja Akhmet Yassawi International Kazakh-Turkish University, Turkestan, Kazakhstan, Second-year master's student, Department of Physics, Spark plasma sintering (SPS); Tungsten carbide-based cemented carbides; Cobalt-free hard alloys
E-mail: berik.kaldar@ayu.edu.kz
ORCID: https://orcid.org/0009-0002-9267-7029